Available online at www.sciencedirect.com
SCIENCE DIRECT®
Tectonophysics 367 (2003) 13–28
TECTONOPHYSICS
www.elsevier.com/locate/tecto

The anisotropy of magnetic susceptibility in biotite, muscovite and chlorite single crystals

Fátima Martín-Hernández*, Ann M. Hirt

Institute of Geophysics, ETH-Hönggerberg, CH-8093 Zürich, Switzerland

Received 27 June 2002; accepted 19 March 2003

Abstract

The anisotropy of magnetic susceptibility (AMS) of single crystals of biotite, muscovite and chlorite has been measured in order to provide accurate values of the magnetic anisotropy properties for these common rock-forming minerals. The low-field AMS and the high-field paramagnetic susceptibility are defined. For the high-field values, it is necessary to combine the paramagnetic deviatoric tensor obtained from the high-field torque magnetometer with the paramagnetic bulk susceptibility measured from magnetization curves of the crystals. This leads to the full paramagnetic susceptibility ellipsoid due to the anisotropic distribution of iron cations in the silicate lattice. The ellipsoid of paramagnetic susceptibility, which was obtained for the three phyllosilicates, is highly oblate in shape and the minimum susceptibility direction is subparallel to the crystallographic *c*-axes. The anisotropy of the susceptibility within the basal plane of the biotite has been evaluated and found to be isotropic within the accuracy of the instrumental measurements. The degree of anisotropy of biotite and chlorite is compatible with previously reported values while for muscovite is smaller than previously published values. The shape of the chlorite AMS ellipsoid for all the samples is near-perfect oblate in contrast with a wide distribution of oblate and prolate values reported in earlier studies. Reliable values are important for deriving models of the magnetic anisotropy where it reflects mineral fabrics and deformation of rocks.

Keywords: Biotite; Muscovite; Chlorite; Paramagnetic and anisotropy of magnetic susceptibility (AMS)

1. Introduction

Phyllosilicates, and in particular micas, are common rock-forming minerals in a large variety of rocks, especially shales and slates. In addition, they are the carriers of the AMS in many of these rocks (Borradaile et al., 1985/86; Hirt et al., 1993, 2000; Lüneburg et al., 1999). To understand the source of the anisotropy of magnetic susceptibility (AMS) in these rocks, several investigations have tried to model the anisotropy of magnetic susceptibility based on the orientation of the main rock-forming minerals and their intrinsic AMS (Siegesmund et al., 1995; de Wall et al., 2000). The AMS of individual minerals, however, is not well constrained with respect to the shape of the AMS ellipsoid or the degree of anisotropy (Borradaile et al., 1987; Zapletal, 1990; Borradaile and Werner, 1994).

* Corresponding author. Present address: Paleomagnetic Laboratory Fort Hoofddijk, Budapestlaan 17, 3584 CD Utrecht, The Netherlands.
E-mail address: fatima@geo.uu.nl (F. Martín-Hernández).

0040-1951/03/$ - see front matter © 2003 Elsevier Science B.V. All rights reserved.
doi:10.1016/S0040-1951(03)00127-6

Phyllosilicates consist of a composite sheet with a layer of $(Si,Al)O_4$ with tetrahedral structure, and a layer of $(Fe,Mg)O_6$ or $(AlO)_6$ with octahedral structure. Individual layers with these two structures stacked in different configurations make up the group of phyllosilicate minerals. The individual sheets are interconnected by van der Waals forces.

Micas, such as biotite and muscovite, form the simplest group of phyllosilicates. The general structure has an octahedral layer between two identical tetrahedral layers, or a 2:1 layer configuration. The general chemical composition of biotite is given by: $K_2(Mg,Fe^{2+})_{6-4}(Fe^{3+},Al,Ti)_{0-2}[Si_{6-5}Al_{2-3}O_{20}](OH,F)_4$ (Deer et al., 1975). However, the composition can vary since biotite forms a continuous chemical and structural series with phlogopite ($K_2(Mg,Fe^{2+})_6[Si_6Al_2O_{20}](OH,F)_4$). In muscovite, which also has a 2:1 layered structure, one quarter of the octahedral sites is occupied by Al and three quarters by Si. The general formula is: $K_2Al_4[Si_6Al_2O_{20}](OH,F)_4$, (Deer et al., 1975). However, Fe^{2+}, Fe^{3+}, Mn^{2+} or Cr^{5+} can also be substituted into the octahedral sites.

Chlorite has a more complicated 2:1:1 structure. It consists of a 2:1 unit sheet with an additional single sheet of cations octahedrally coordinated by hydroxyls. There are multiple variations of the Fe^{2+}, Fe^{3+}, Si or Mg content within the series as well as substitutions or alterations in the layered sequence. The general formula for chlorite according to Deer et al. (1975) is $(Mg,Al,Fe)_{12}[(Si,Al)_8O_{20}](OH)_{16}$.

The first reported values of magnetic properties of micas were determined for the bulk magnetic susceptibility (Syono, 1960; Hood and Custer, 1967). Compositional analysis revealed how the magnetic susceptibility is related to the cation content in the samples. This led to empirical and theoretical formulas that correlate the magnetic cation content with the bulk susceptibility (Rochette, 1987). Later, a temperature dependence was introduced in the formula (Rochette et al., 1992).

Biotite is the phyllosilicate whose magnetic anisotropy is best known. Ballet and Coey (1982) studied the magnetic susceptibility of two biotite crystals. Measurements in two perpendicular planes gave the susceptibilities normal ($k_\perp$) and parallel ($k_\parallel$) to the crystal cleavage. Beausoleil et al. (1983) determined the magnetic behaviour of eight samples of biotite in high fields, finding a susceptibility ratio $k_\perp/k_\parallel \simeq 1.25$ with respect to cleavage. Borradaile et al. (1987) measured the AMS of two biotite oriented aggregates with an induction coil. Using the definitions of Jelinek (1981) for the degree of anisotropy (P_j) and the shape of the anisotropy (T), they found $P_j = 1.40$ and $T = 0.97$. Ten biotite single crystals were measured in low field by Zapletal (1990) with a KLY-2 susceptibility bridge in order to determine a representative value of their magnetic anisotropy. Although the samples were selected because of their low ferromagnetic content, it was shown that they acquired an IRM in fields up to 1 T. Only two crystals, which were free of significant ferrimagnetic inclusions, were considered for the final evaluation of the AMS ellipsoid. The mean value of the anisotropy degree was $P_j = 1.23$ and the shape parameter was $T = 0.95$. Borradaile and Werner (1994) improved the determination of the magnetic anisotropy of biotites by applying high-field methods for the isolation of the paramagnetic component of the anisotropy. In their study, the paramagnetic component of the AMS is calculated from the high-field slope of hysteresis loops; this requires the crystallographic orientation of the samples be well controlled. Twenty-nine crystals were analyzed using this method. A mean anisotropy degree of $P_j = 1.50$ was determined, which is higher than values reported previously. The mean shape factor was found to be $T = 0.69$, less oblate than expected due to the presence of some samples that had prolate ellipsoids.

Magnetic properties of muscovite have been presented by Ballet and Coey (1982). They characterized the paramagnetic Curie temperature and Curie constant in two orthogonal directions, parallel and perpendicular to the crystal cleavage plane, respectively. Borradaile et al. (1987) reported a single value of the AMS for a crystal of muscovite, in which the anisotropy degree found was $P_j = 1.43$ and the shape parameter $T = 0.44$. Borradaile and Werner (1994), analyzing the anisotropy of the paramagnetic susceptibility using hysteresis loops, obtained a broad variability of values, which included prolate anisotropies. The average ellipsoid was characterized by an anisotropy degree $P_j = 1.29$ and a shape parameter of $T = 0.63$. A total of 18% of the muscovite crystals were reported as having the k_3 axes lying within the basal plane.

Little work has been done on the determination of the magnetic anisotropy of chlorite. Ballet et al. (1985) reported on the anisotropy of the magnetic susceptibility, where they found a positive paramagnetic Curie temperature in the basal plane and a negative value perpendicular to the basal plane. Borradaile et al. (1987) examined four single crystals of chlorite with an induction coil instrument. They reported mean values of $P_j = 1.38$ and $T = 0.43$. Borradaile and Werner (1994) analyzed 42 specimens using hysteresis loops for the separation of the paramagnetic component. They found a value of $P_j = 1.33$ and an ellipsoid with a mean shape almost neutral with $T = 0.33$ due to some samples with prolate ellipsoid. About 30% of the samples showed minimum susceptibility axes in the basal plane.

In this study, a collection of biotite, muscovite and chlorite samples has been measured on a high-field torque magnetometer that allows the separation of the paramagnetic and ferrimagnetic components of the AMS. This method is suitable for single crystals of phyllosilicates because it allows the calculation of the crystal paramagnetic component of magnetic anisotropy and does not require a priori assumptions about the orientation of the susceptibility ellipsoid. We present new reliable values of the AMS for biotite, muscovite and chlorite, which can be used for modelling of the magnetic fabrics of rocks. Reliable models are necessary to understand how AMS reflects deformation so that magnetic measurements can serve as a proxy for rock deformation.

2. Experimental method

2.1. Sample description

A collection of single crystals, including seven biotites, five muscovites and six chlorites from different localities, were analyzed. A number of specimens from each crystal were cut with a ceramic knife. The individual specimens had a rectangular shape and were mounted in plastic boxes with non-magnetic glue. The samples were oriented in the holder so that the crystallographic *c*-axis lies flat, parallel to a basal edge of the box.

2.2. Measurement procedure

Two different types of measurements have been made: measurement of the susceptibility in both low and high fields, and measurement of remanence in order to independently characterize the ferromagnetic phases. The low-field anisotropy of magnetic susceptibility was measured on an AGICO KLY-2 susceptibility bridge in an applied field of 300 A/m (Tarling and Hrouda, 1993). Fifteen independent measurement positions are used to define the six components of the symmetric susceptibility tensor (Jelinek, 1978). The eigenvalues of the susceptibility tensor lead to the determination of a susceptibility ellipsoid with principal axes $k_1 \geq k_2 \geq k_3$. The shape and degree of anisotropy of the AMS ellipsoid have been characterized by the T parameter and the corrected degree of anisotropy P_j, respectively (Jelinek, 1981).

The high-field anisotropy has been measured on a high-field torque magnetometer, operating with a maximum applied field of 1.85 T (Bergmüller et al., 1994). The samples were measured in four fields (1.2, 1.4, 1.6 and 1.8 T) that are high enough to saturate the ferrimagnetic inclusions in the crystal. The processing of the torque signal allows separation of the paramagnetic and ferromagnetic components, using the method reported by Martín-Hernández and Hirt (2001). The percentage of the individual components is defined from the deviatoric susceptibility tensor due to the paramagnetic and ferromagnetic contribution to the torque signal. In order to define the full paramagnetic tensor, the paramagnetic susceptibility is needed. Therefore, a small chip was cut from each crystal to evaluate the paramagnetic bulk susceptibility, defined as the slope of the magnetization curve above the saturation of the ferromagnetic minerals. Magnetization curves were measured with a maximum field of 1.8 T on a PCM-VSM at the Institute of Rock Magnetism, University of Minnesota. Three mutually perpendicular measurements were made to estimate the mean bulk paramagnetic susceptibility for each specimen, and specimen susceptibilities were averaged to obtain a mean value per crystal. One measurement was always subparallel to the crystalline *c*-axis and the other two within the basal plane of the crystal. The bulk susceptibility is added to the deviatoric paramagnetic tensor in order to compute the full paramagnetic tensor. Both the low-field AMS and the

high-field paramagnetic tensor were normalized with the criterion $k_1+k_2+k_3=3$. The magnetic susceptibility ellipsoid is represented on a Jelinek plot showing the ellipsoid shape as a function of its degree of anisotropy (Jelinek, 1981).

In order to identify the ferromagnetic phases in the crystals, the progressive acquisition of isothermal remanent magnetization (IRM) was observed in fields up to 1 T, produced by an electromagnet. The shape of the acquisition curves is dependent on the type of ferromagnetic minerals. The maximum coercivities of the common ferromagnetic minerals are well known which aids in their identification (cf., Dunlop and Özdemir, 1997).

The magnetization of biotite and muscovite has been also studied at low temperature for identification of ferrimagnetic inclusions, using a Quantum Design MPMS2 susceptometer at the Institute of Rock Magnetism, University of Minnesota. The experiment consists of measuring the magnetization when the sample is cooled down in zero field to 50 K after magnetizing it at room temperature with a saturating field of 2.5 T. The magnetization is subsequently observed during warming up in zero field between 50 and 300 K.

Mössbauer spectroscopy has been used already by several authors as a suitable method for estimating the Fe^{2+}/Fe^{3+} in micas (Ballet and Coey, 1982; Townsend and Longworth, 1985; Zapletal, 1990). Variations in the iron content contribute to the differences in bulk susceptibility (Rochette, 1987). Mössbauer spectra were measured for four biotite crystals. The samples were reduced to powder and measured on a Ranger Scientific Mössbauer Spectrometer with a radioactive ^{57}Co source at the Institute of Rock Magnetism, University of Minnesota. A least squares fit with three Lorentian shape doublets was used to identify the presence of ferrous octahedral cations [Fe^{2+}], ferric octahedral cations [Fe^{3+}] and tetrahedral ferric cations $\langle Fe^{3+}\rangle$ (Rancourt, 1998).

3. Biotite single crystals

3.1. Ferrimagnetic phases

In order to identify the ferrimagnetic phases present in biotite crystals, IRM acquisition curves were measured on one specimen from each crystal. The results show the presence of a low coercivity phase that saturates around 300 mT (Fig. 1a). The same low coercivity phase has been found systematically in all the crystals. The presence of a low coercivity phase in biotite crystals has been pointed out earlier by Zapletal (1990) and Borradaile and Werner (1994).

The low temperature remanence experiments on the biotite crystals show a drop in the magnetization upon cooling between 130 and 105 K (Fig. 1b). This may be due to the magnetite Verwey transition (Verwey, 1939) or cooling through the magnetite isotropic point (Muxworthy, 1999). The magnetization decrease indicates the presence of pure multidomain magnetite or interacting single domain grains.

3.1.1. Mössbauer spectrometry

A Mössbauer spectrum was measured for each of four biotite crystals at room temperature in order to analyze possible variations in the Fe^{2+}/Fe^{3+} content. None of the samples shows signs of hyperfine splitting that would indicate the presence of ferrimagnetic phases (Fig. 2).

The spectra are characterized by three main doublets due to the presence of octahedrally coordinated Fe^{2+} in the silicate lattice and both octahedrally and tetrahedrally coordinated Fe^{3+}. The isomer shifts (δ) and their quadrupole splitting (Δ) have been used to identify the nature and location of the cations (Rancourt, 1998). The values obtained are summarized in Table 1.

In the specific case of biotite, the ratio of subtended areas for the Lorentian fitting functions is proportional to the ratio of populations because there is no recoilless fraction of the nuclei (Lalonde et al., 1998). The Fe^{2+}/Fe^{3+} ratio of the analyzed biotites is summarized in Table 1. The Fe^{2+} content is variable between specimens and dominates over the Fe^{3+} cations.

3.2. Low-field magnetic anisotropy susceptibility of biotite

Normalized principal axes of the AMS ellipsoid, shape and degree of anisotropy for the biotite specimens are summarized in Table 2. The values obtained show an oblate mean ellipsoid as seen from the positive T parameter ranging from 0.75 to 0.99 (Fig. 3). The anisotropy degree P_j has a larger scatter,

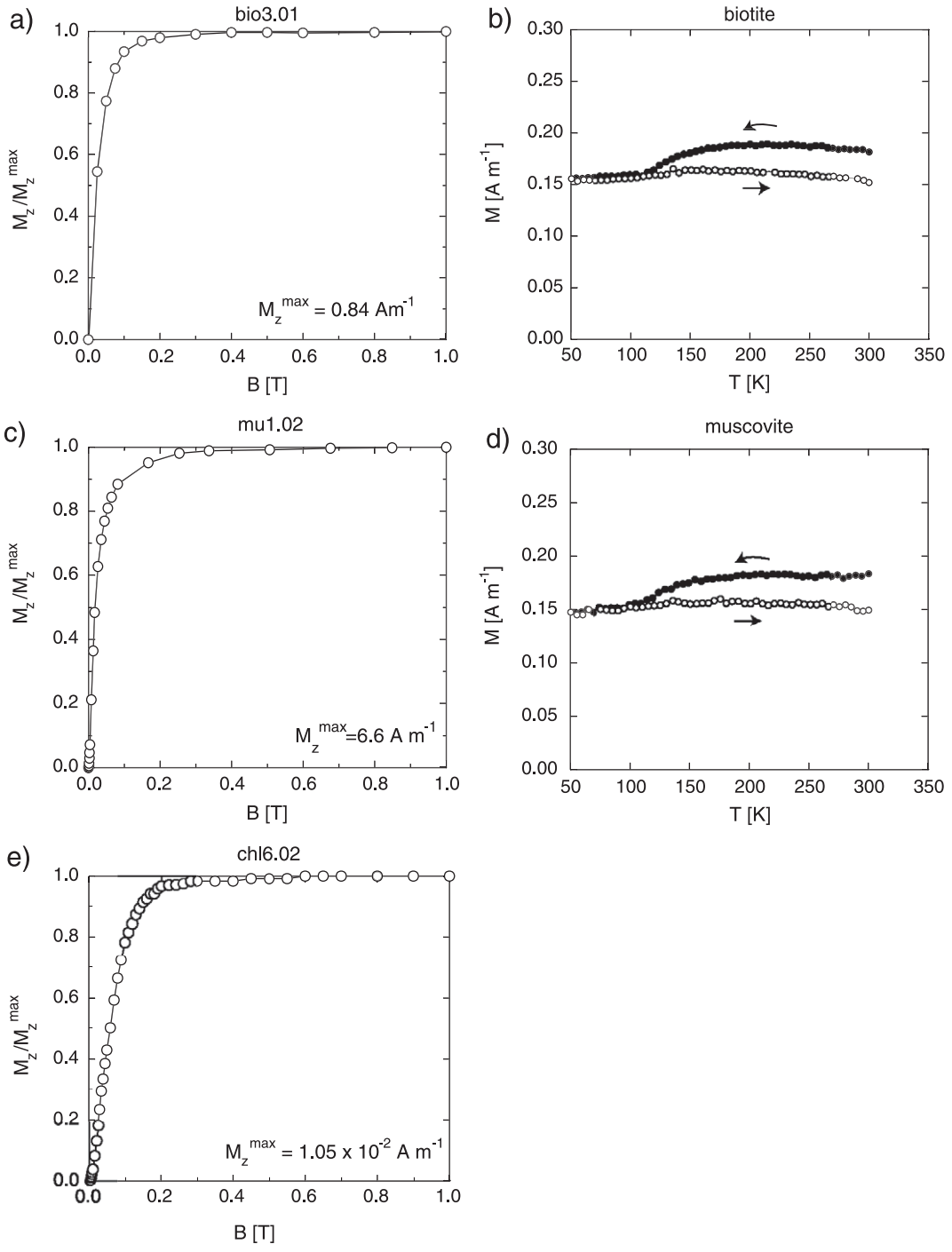

Fig. 1. Remanence experiments to identify ferrimagnetic inclusions. IRM acquisition curves with the field applied in the basal plane (left) and low temperature remanence experiment of a zero-field cooling curve of the SIRM and subsequent zero-field warming curve (right). (a, b) Biotite single crystal, (c, d) muscovite single crystal, and (e) chlorite single crystal.

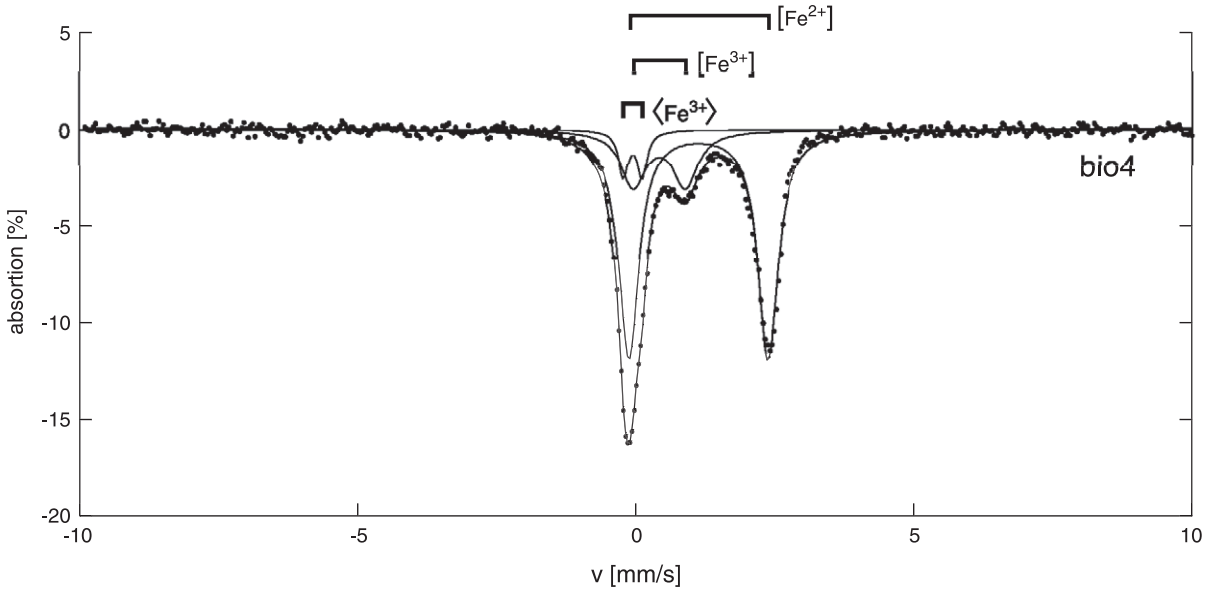

Fig. 2. Mössbauer spectra of biotite powder sample bio4. Dots correspond to the measurements, the curves correspond to the best fit Lorentzian function where $\langle Fe^{3+}\rangle$ corresponds to tetrahedrally coordinated ferric cations, $[Fe^{3+}]$ to octahedrally coordinate ferric cations, and $[Fe^{2+}]$ to octahedrally coordinate ferrous cations.

especially in sample bio1.02, which has a higher value of 1.47. However, these results are in good agreement with values previously reported by low-field methods (Borradaile et al., 1987; Zapletal, 1990).

3.3. High-field magnetic susceptibility anisotropy of biotite

Twelve biotite samples have been measured on a high-field torque magnetometer to obtain the paramagnetic and ferrimagnetic contributions to the magnetic anisotropy. The samples were oriented with the *y*-direction subparallel to the *c*-axes of the phyllosilicate and with the *x*-direction and *z*-direction contained within the basal plane. The magnetic torques in the two planes perpendicular to the crystal cleavage are dominated by the 2θ-term (Fig. 4a). The torque signal in the basal plane is very weak and therefore some of the torque curves are not perfectly symmetric, but with a clear 2θ dependency (Fig. 4c).

Table 1
Mössbauer data for the biotite samples

Sample	Site	δ (mm/s)	Δ (mm/s)	Fe^{2+} (%)	Fe^{2+}/Fe^{3+}
bio1	$[Fe^{2+}]$	1.143	2.416	81	3.4
	$[Fe^{3+}]$	0.335	0.992		
	$\langle Fe^{3+}\rangle$	−0.021	0.336		
bio2	$[Fe^{2+}]$	1.140	2.421	74	3.0
	$[Fe^{3+}]$	0.288	1.026		
	$\langle Fe^{3+}\rangle$	−0.007	0.303		
bio4	$[Fe^{2+}]$	1.129	2.495	77	2.5
	$[Fe^{3+}]$	0.430	0.929		
	$\langle Fe^{3+}\rangle$	−0.047	0.337		
bio5	$[Fe^{2+}]$	1.142	2.415	87	3.7
	$[Fe^{3+}]$	0.345	0.978		
	$\langle Fe^{3+}\rangle$	−0.015	0.371		

The 2θ-term of the torque signal is proportional to B^2 in the three planes (Fig. 4b and d). The intercept of the straight line that fits the 2θ-term as a function of B^2 was not statistically significant at the 95% level of confidence, as computed with the aid of the Student *t* statistic (Cheeney, 1983). The absence of a significant nonzero intercept of the straight line shows that the anisotropy is carried by the paramagnetic phase. The ferrimagnetic fraction is not significant; the error of measurements is larger than the ferrimagnetic percentage (Table 2). The deviatoric paramagnetic susceptibility tensor was computed after separating the different magnetic components from the torque signal. The principal directions of

Table 2
Magnitudes and directions of the principal AMS axes

Name	k_1^{LF}	k_2^{LF}	k_3^{LF}	k_{bulk}^{LF} (S.I.)	P_j^{LF}	T^{LF}	k_1^{para}	k_2^{para}	k_3^{para}	k_{bulk}^{para} (S.I.)	P_j^{para}	T^{para}	%para.	%ferro.
bio1.01(1)	1.091	1.062	0.848	1.35×10^{-3}	1.32	0.79	1.079	1.072	0.850	1.29×10^{-3}	1.31	0.94	96 ± 6	4 ± 4
bio1.02(1)	1.127	1.079	0.794	0.98×10^{-3}	1.47	0.75	1.079	1.072	0.848	1.29×10^{-3}	1.32	0.95	96 ± 5	4 ± 5
bio1.03(1)	1.084	1.078	0.838	1.02×10^{-3}	1.34	0.95	1.073	1.065	0.861	1.29×10^{-3}	1.28	0.93	96 ± 5	4 ± 4
bio1.04(1)	1.090	1.064	0.845	1.22×10^{-3}	1.32	0.81	1.079	1.073	0.848	1.29×10^{-3}	1.32	0.95	94 ± 7	6 ± 6
bio2.01(1)	1.093	1.080	0.827	1.04×10^{-3}	1.37	0.91	1.082	1.076	0.843	1.25×10^{-3}	1.33	0.95	94 ± 7	6 ± 6
bio2.02(1)	1.092	1.083	0.825	1.10×10^{-3}	1.37	0.94	1.080	1.076	0.844	1.25×10^{-3}	1.33	0.97	94 ± 6	6 ± 6
bio4.01(2)	1.104	1.084	0.812	0.74×10^{-3}	1.41	0.88	1.052	1.052	0.896	1.36×10^{-3}	1.20	1.00	94 ± 8	6 ± 6
bio5.01(1)	1.087	1.067	0.846	1.13×10^{-3}	1.32	0.86	1.089	1.082	0.829	1.13×10^{-3}	1.36	0.96	99 ± 12	1 ± 3
bio6.01(3)	1.084	1.073	0.844	1.10×10^{-3}	1.33	0.92	1.084	1.079	0.836	1.20×10^{-3}	1.35	0.97	94 ± 15	6 ± 8
bio6.02(3)	1.074	1.074	0.852	1.09×10^{-3}	1.31	0.99	1.077	1.073	0.851	1.20×10^{-3}	1.31	0.97	94 ± 8	6 ± 6
bio7.02(1)	1.081	1.075	0.844	1.00×10^{-3}	1.33	0.96	1.073	1.067	0.860	1.20×10^{-3}	1.29	0.96	99 ± 5	1 ± 3
bio7.04(1)	1.045	1.035	0.920	1.14×10^{-3}	1.15	0.86	1.083	1.076	0.841	1.20×10^{-3}	1.34	0.95	99 ± 5	1 ± 2
mean	1.09 ± 0.02	1.07 ± 0.02	0.84 ± 0.03	$1.07 \times 10^{-3} \pm 0.10 \times 10^{-3}$	1.34 ± 0.07	0.88 ± 0.07	1.08 ± 0.01	1.07 ± 0.01	0.85 ± 0.02	$1.25 \times 10^{-3} \pm 0.06 \times 10^{-3}$	1.31 ± 0.04	0.96 ± 0.02		

The table shows low-field data (LF), magnetic susceptibility of the paramagnetic fraction (para) measured on a high-field torque magnetometer, and percentages of paramagnetic and ferrimagnetic anisotropic components in the high-field AMS. Superindexes in the sample name indicate the origin of the analyzed crystals. (1) Bancroft, Canada, (2) Swiss Alps and (3) Bear Lake, Canada. Mean values of P_j and T and their standard deviation are based on individual P_j and T values for this and subsequent tables.

the paramagnetic susceptibility tensor are consistent with the crystallographic structure of the phyllosilicates, with the k_3 semiaxes subparallel to the c-axes of the crystal and the k_1 and k_2 axes contained within the basal plane.

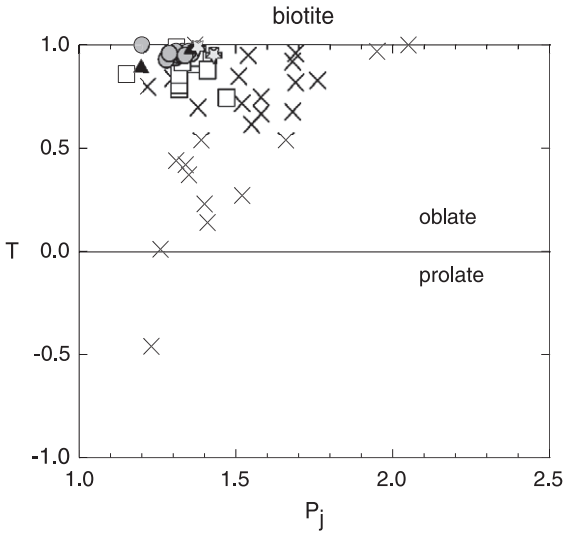

Fig. 3. Jelinek plot of the magnetic susceptibility ellipsoid for single crystals of biotite. Gray stars represent data from Borradaile et al. (1987), black triangles represent data from Zapletal (1990), crosses represent data from Borradaile and Werner (1994), open squares are low-field values, and gray circles the paramagnetic anisotropy derived from torque measurements from this study in this and subsequent figures.

The magnetization curve shows an almost pure paramagnetic signal (Fig. 5a) after correction for the sample holder signal. After removing the paramagnetic susceptibility defined from the linear slope above 0.9 T, the remaining signal reveals the presence of traces of ferrimagnetic phases. The signal is poor and noisy, but can be recognized as a hysteresis loop due to a ferrimagnetic phase (Fig. 5a). The bulk susceptibility of the paramagnetic fraction was defined as the mean value from the three measurements (Table 2). For each crystal an arithmetic mean is calculated from the specimen susceptibilities in order to estimate the mean bulk susceptibility. These values were used to compute the full paramagnetic tensor (Table 2).

3.3.1. High-field magnetic susceptibility of biotite in the basal plane

There is some ambiguity as to whether magnetic susceptibility within the basal plane of mica is isotropic. The paramagnetic anisotropy is highly oblate, $T = 0.96 \pm 0.02$. However, in some studies, the minimum susceptibility was reported to deviate 5° with respect to the crystallographic c-axis; this was attributed to the location of the cations in the octahedral sites of the stacked sheets (Borradaile and

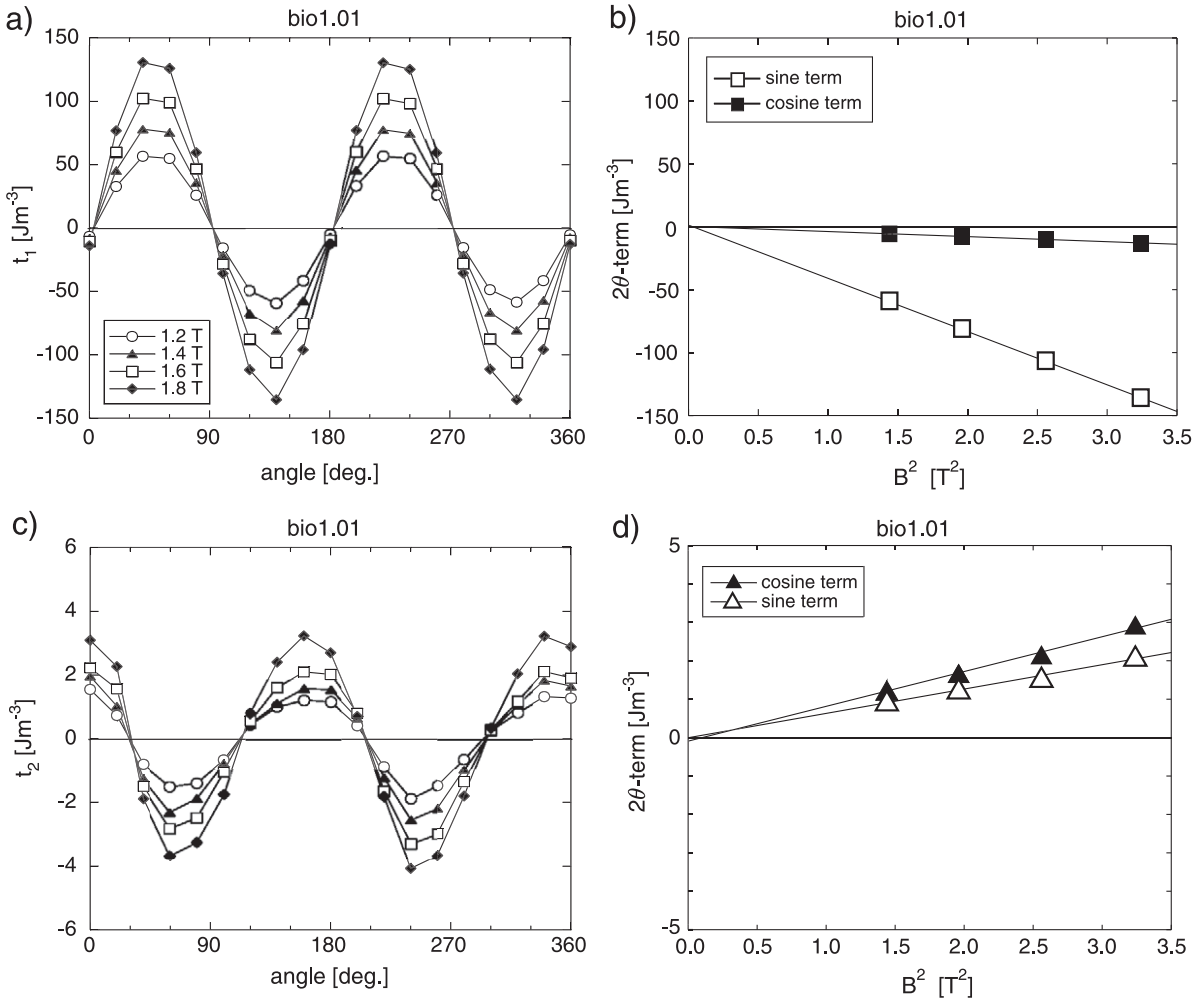

Fig. 4. (a) Torque per unit volume as a function of measurement angle in the plane *xy* perpendicular to cleavage in a biotite single crystal (b) and amplitude of the 2θ-term as a function of B^2 on the same plane. (c) Torque per unit volume as a function of measurement angle within the crystal cleavage plane and (d) amplitude of the 2θ-term as a function of B^2 on the same plane.

Werner, 1994). Ballet and Coey (1982) considered the direction normal to the basal plane as the hard direction of susceptibility. In order to check for possible anisotropy in the basal plane of biotite, the magnetic susceptibility has been determined as a function of orientation in one sample per crystal. The samples were measured on a VSM at 10° intervals from 0° to 360°. The holder used was especially designed to be as perpendicular as possible to the head of the instrument to avoid mis-

Fig. 5. Magnetization curves of a studied phyllosilicate single crystal with the field applied in a direction within the basal plane. Linear relationship between applied field and magnetization and weak ferrimagnetic signal after subtraction of the paramagnetic component (right) and hysteresis loop in samples with a strong ferrimagnetic signal after subtraction of the paramagnetic signal (left). The inset shows the signal after subtraction of the paramagnetic component assuming saturation at 50% below maximum field. (a) Biotite single crystal, (b, c) muscovite single crystal, and (d, e) chlorite single crystal.

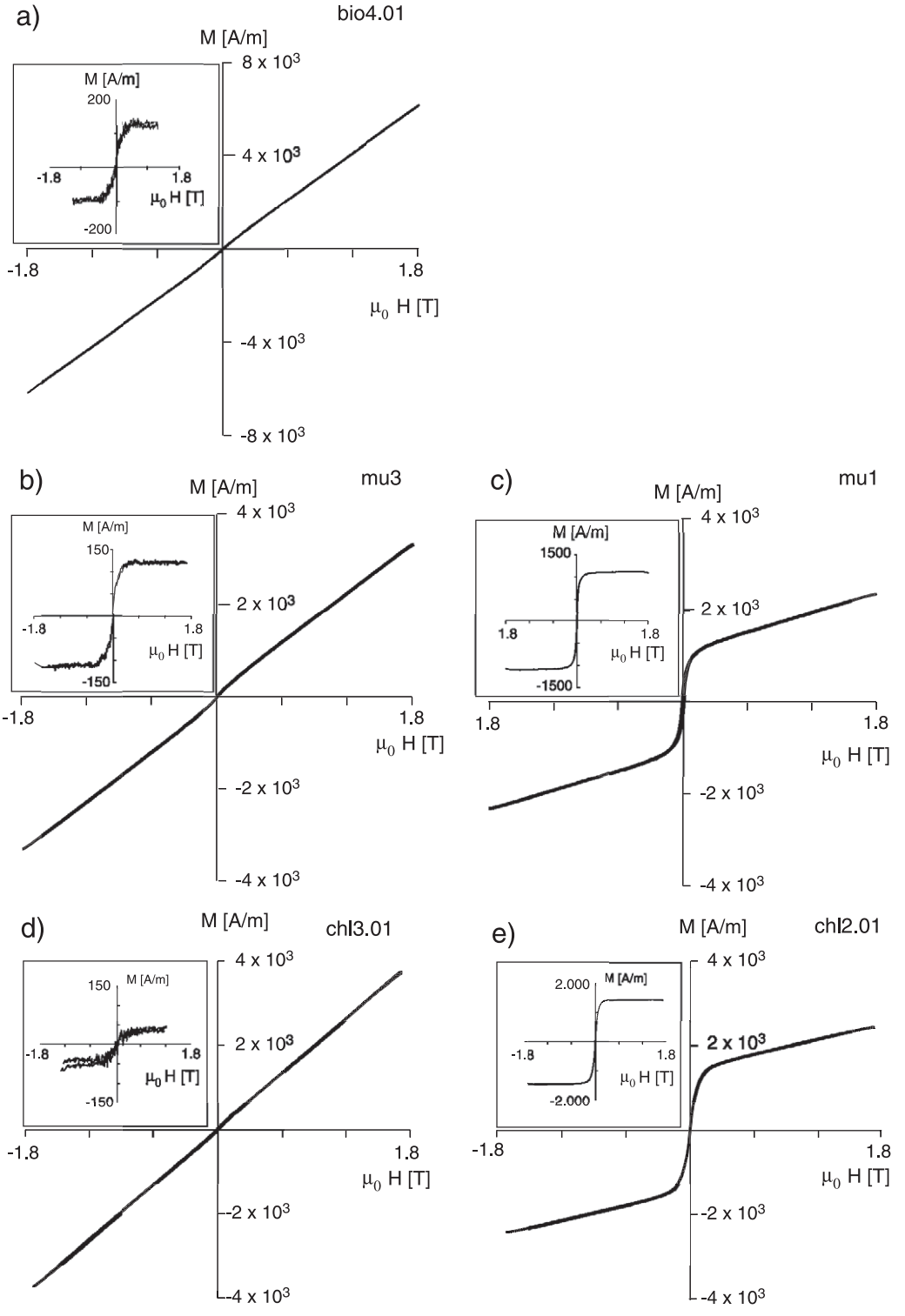
a)
bio4.01
M [A/m]
8 x 10^3
4 x 10^3
-4 x 10^3
-8 x 10^3
-1.8
1.8
μ0 H [T]
M [A/m]
200
-200
b)
mu3
c)
mu1
1500
-1500
d)
chl3.01
150
-150
e)
chl2.01
2.000
-2.000
2 x 10^3
-2 x 10^3

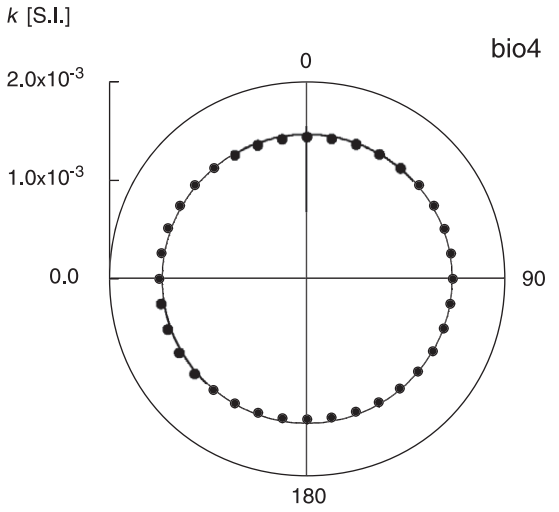

Fig. 6. Paramagnetic susceptibility of a biotite crystal in the basal plane. Solid line represents the best-fit centered circle to the magnetic susceptibility and full circles represent measured values.

orientation with respect to the basal plane. The directional magnetic susceptibility has been represented as a function of orientation in Fig. 6. The residual values between the best-fit circle and the data ranged between 1.4% in sample bio4 and 3% in sample bio2. It is not possible to distinguish whether the deviation from a circle is due to an anisotropy or from a possible misorientation of the crystal in the instrument. However, any basal-plane anisotropy must be very small, at more than a few percent.

4. Muscovite single crystals

4.1. Ferrimagnetic phases

IRM acquisition curves have been made for one specimen from each crystal of muscovite. The curves reveal the systematic presence of a low coercivity phase that acquires a magnetization at very low coercivities and is nearly saturated at 300 mT. An additional higher coercivity phase is also present that does not saturate at 1 T (Fig. 1c). The presence of pseudo-single domain magnetite in muscovite has been reported by Borradaile and Werner (1994), but there was not evidence of a high coercivity phase in any previous study.

The saturation isothermal magnetization (SIRM) in muscovite shows a decrease at about 130 K during zero-field cooling (Fig. 1d). Upon warming the magnetization is not recovered. This behaviour is indicative of pure magnetite.

4.2. Low-field magnetic anisotropy susceptibility of muscovite

The results of the low-field AMS of the muscovite crystals are summarized in Table 3. The dispersion of the degree of anisotropy is high, especially for the specimen of crystal mu1 with a value of 2.41 that is close to twice that of the other crystals. The darker color of the samples suggests that the crystals are not pure muscovite or that they have

Table 3
Magnitudes and directions of the principal AMS axes for the muscovite crystals

Name	k_1^{LF}	k_2^{LF}	k_3^{LF}	k_{bulk}^{LF} (S.I.)	P_j^{LF}	T^{LF}	k_1^{para}	k_2^{para}	k_3^{para}	k_{bulk}^{para} (S.I.)	P_j^{para}	T^{para}	%para.	%ferro.
mu1.01(2)	1.334	1.092	0.575	4.02×10^{-4}	2.41	0.52	1.041	1.031	0.928	2.64×10^{-4}	1.14	0.83	57 ± 11	43 ± 14
mu2.01(4)	1.092	1.055	0.853	0.77×10^{-4}	1.31	0.72	1.073	1.045	0.882	1.00×10^{-4}	1.24	0.73	92 ± 9	8 ± 10
mu2.02(4)	1.121	1.009	0.869	0.79×10^{-4}	1.29	0.17	1.026	1.017	0.957	2.80×10^{-4}	1.08	0.77	95 ± 10	5 ± 6
mu2.03(4)	1.125	1.061	0.814	0.65×10^{-4}	1.41	0.64	1.025	1.016	0.959	2.80×10^{-4}	1.07	0.75	89 ± 10	11 ± 30
mu3.01(4)	1.122	1.074	0.804	1.18×10^{-4}	1.44	0.73	1.053	1.044	0.902	2.20×10^{-4}	1.19	0.89	94 ± 8	6 ± 6
mu3.02(4)	1.106	1.068	0.825	1.16×10^{-4}	1.38	0.76	1.046	1.037	0.917	2.60×10^{-4}	1.16	0.88	94 ± 6	6 ± 6
mu3.03(4)	1.111	1.079	0.810	1.15×10^{-4}	1.42	0.81	1.044	1.038	0.918	2.65×10^{-4}	1.16	0.90	94 ± 5	6 ± 6
mu4.01(4)	1.106	1.076	0.818	1.18×10^{-4}	1.40	0.82	1.036	1.031	0.933	3.38×10^{-4}	1.12	0.91	94 ± 6	6 ± 6
mu5.01(4)	1.088	1.085	0.827	1.26×10^{-4}	1.37	0.98	1.055	1.046	0.899	2.54×10^{-4}	1.20	0.89	94 ± 8	6 ± 6
mean	1.13 ± 0.08	1.07 ± 0.02	0.80 ± 0.09	$1.10 \times 10^{-4} \pm 1.11 \times 10^{-4}$	1.49 ± 0.35	0.68 ± 0.23	1.04 ± 0.01	1.03 ± 0.01	0.92 ± 0.03	$2.5 \times 10^{-4} \pm 0.6 \times 10^{-4}$	1.15 ± 0.05	0.84 ± 0.08		

The table shows low-field data (LF), magnetic susceptibility of the paramagnetic fraction (para) measured on a high-field torque magnetometer, and the percentages of the paramagnetic and ferrimagnetic anisotropic fractions. Superindexes in the sample name indicate the origin of the analyzed crystals. (2) Swiss Alps and (4) Madras, India.

a high concentration of ferrimagnetic inclusions. The shape of the susceptibility ellipsoid is also scattered with values that range from 0.17, almost neutral in shape, to 0.98, close to oblate shape (Fig. 7).

4.3. High-field magnetic anisotropy susceptibility of muscovite

Nine muscovite samples have been measured on a high-field torque magnetometer to obtain the paramagnetic and ferrimagnetic contributions to the magnetic anisotropy. The torque signal in a plane perpendicular to the crystal cleavage is similar to that in biotite single crystals, although with lower intensity because the susceptibility is lower. The torque signal within the basal plane is also characterized by a significant contribution of the 2θ-term.

Sample from crystal mu1 has a statistically significant ferrimagnetic fraction, represented by a non-zero intercept of the line that fits the 2θ-term of the Fourier analysis as a function of the square of applied field. After separation of the magnetic components, the fraction of anisotropic ferrimagnetic minerals is significant in the sample from this crystal (Table 3).

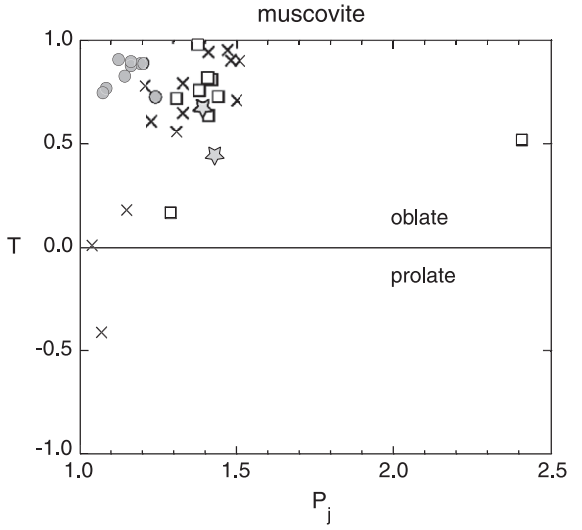

Fig. 7. Jelinek plot of the magnetic susceptibility ellipsoid for single crystals of muscovite.

The magnetization curves, measured in order to calculate the paramagnetic bulk susceptibility, also have a measurable ferromagnetic component. Samples with an insignificant ferrimagnetic fraction show a linear relationship between applied field and magnetization (Fig. 5b). The intensity of the magnetizations is very weak in these specimens, so that three curves were stacked in order to define the paramagnetic susceptibility.

Samples from crystal mu1 exhibit a closed hysteresis loop that reaches saturation at 300 mT (Fig. 5c). The bulk susceptibility obtained from both types of sample is on the same order of magnitude and was combined with the deviatoric paramagnetic susceptibility tensor to obtain the full paramagnetic susceptibility ellipsoid (Fig. 7 and Table 3).

The paramagnetic ellipsoid obtained is highly oblate, as it has been already reported. The degree of anisotropy is slightly smaller than the data available in the literature. However, the obtained values show that muscovite has a smaller degree of anisotropy because Fe is a substitution product and a cation forming the general structure of the muscovite lattice.

5. Chlorite single crystals

5.1. Ferrimagnetic phases

The IRM acquisition curve of a chlorite crystal shows the presence of a low coercivity phase that almost saturates at 300 mT; it is most likely magnetite (Fig. 1e). The study done by Borradaile and Werner (1994) also showed a ferromagnetic phase in chlorites, which they found to be compatible with pseudo-single domain or multidomain magnetite. A second phase with a higher coercivity may also be present in chlorite samples: the presence of hematite in chlorite samples has been reported previously from high-field torque magnetometer analysis (Parry, 1971). Significant amounts of hematite would falsify any analysis of the high-field torque curves since its torque is dependent on B and not on B^2 (Porath and Chamalaun, 1966). Therefore, any sample with a high-coercivity component in IRM acquisition has been omitted from further study at this time.

Chlorite samples were not available for low temperature remanence experiments.

5.2. Low-field magnetic susceptibility anisotropy of chlorite

The low-field anisotropy results are given in Table 4. The dispersion of the data is high, especially in the determination of the shape of the AMS ellipsoid, which has a mean value of $T=0.63$ that is moderately oblate (Fig. 8). The range of values in the bulk susceptibility is broad, suggesting the presence of ferromagnetic phases, which increase the susceptibility value.

5.3. High-field magnetic susceptibility anisotropy of chlorite

Eight specimens from six different crystals have been measured with the high-field torque magnetometer. The torque signal in a plane perpendicular to the crystal cleavage shows the same behaviour as the biotite and muscovite single crystals. The torque is characterized by a trigonometric function depending on 2θ, with lower intensity than the torque of biotite, but similar to muscovite, depending on the susceptibility of the crystals. Similar behaviour is also found in the measurements within the basal plane, with a significant 2θ-term of the signal of weaker intensities than in the other two planes. The Fourier 2θ-term of all measured planes shows a linear relationship with B^2. The separation of the magnetic components of the AMS reveals that ferromagnetic phases contribute to the magnetic anisotropy in only three of the measured specimens (Table 4).

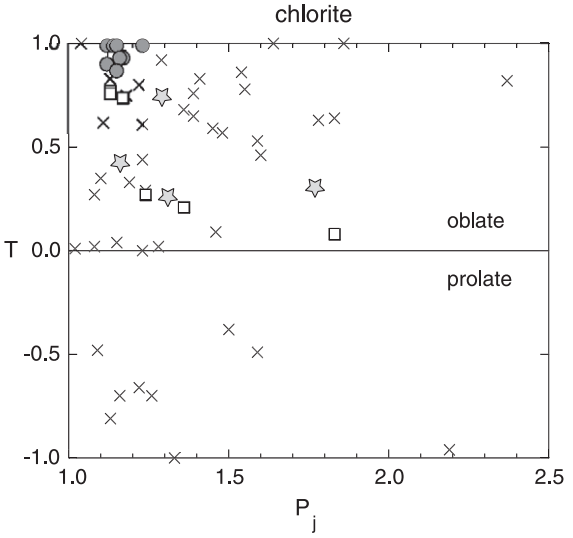

Fig. 8. Jelinek plot of the magnetic susceptibility ellipsoid for single crystals of chlorite.

The magnetization curves measured in chlorite single crystals show a linear dependence of the magnetization on the applied field in general (Fig. 5d). Only in samples with a significant ferrimagnetic contribution to the high-field AMS does the curve show hysteresis (Fig. 5e). After paramagnetic correction of the loop, the curve reveals the presence of a ferrimagnetic phase that saturates at about 300 mT, which together with the IRM acquisition suggests the presence of magnetite (Figs. 1e and 5e).

Fig. 8 shows the anisotropy parameters obtained for the full paramagnetic AMS of analyzed chlorites

Table 4
Magnitudes and directions of the principal AMS axes for the chlorite crystals

Name	k_1^{LF}	k_2^{LF}	k_3^{LF}	k_{bulk}^{LF} (S.I.)	P_j^{LF}	T^{LF}	k_1^{para}	k_2^{para}	k_3^{para}	k_{bulk}^{para} (S.I.)	P_j^{para}	T^{para}	%para.	%ferro.
chl1.01(2)	1.052	1.033	0.914	2.1×10^{-4}	1.17	0.74	1.046	1.041	0.912	2.26×10^{-4}	1.17	0.93	94 ± 9	5 ± 7
chl1.02(2)	1.042	1.028	0.930	2.2×10^{-4}	1.13	0.77	1.034	1.029	0.938	2.75×10^{-4}	1.12	0.90	94 ± 6	6 ± 6
chl2.01(2)	1.303	0.986	0.711	13.9×10^{-4}	1.83	0.08	1.031	1.031	0.938	3.16×10^{-4}	1.12	0.99	62 ± 3	38 ± 4
chl3.01(2)	1.044	1.040	0.916	2.4×10^{-4}	1.16	0.94	1.059	1.058	0.883	1.95×10^{-4}	1.23	0.99	94 ± 10	6 ± 6
chl4.01(2)	1.142	1.014	0.844	4.1×10^{-4}	1.36	0.21	1.037	1.037	0.925	2.45×10^{-4}	1.14	0.99	90 ± 9	10 ± 8
chl5.01(2)	1.040	1.027	0.933	2.5×10^{-4}	1.13	0.76	1.040	1.039	0.921	2.52×10^{-4}	1.15	0.99	94 ± 8	5 ± 5
chl5.02(2)	1.040	1.037	0.924	2.3×10^{-4}	1.14	0.95	1.044	1.039	0.917	2.52×10^{-4}	1.16	0.93	93 ± 8	7 ± 8
chl6.01(2)	1.099	1.016	0.886	9.6×10^{-4}	1.24	0.27	1.042	1.034	0.923	2.45×10^{-4}	1.15	0.87	86 ± 8	14 ± 10
mean	1.10 ± 0.09	1.02 ± 0.02	0.88 ± 0.08	$4.9\times10^{-4}\pm4.4\times10^{-4}$	1.30 ± 0.27	0.63 ± 0.31	1.04 ± 0.01	1.04 ± 0.01	0.92 ± 0.02	$2.51\times10^{-4}\pm0.3\times10^{-4}$	1.15 ± 0.04	0.95 ± 0.05		

The table shows low-field data (LF), magnetic susceptibility of the paramagnetic fraction (para) measured on a high-field torque magnetometer, and the percentage of the paramagnetic and ferrimagnetic anisotropic fractions. Superindexes in the sample name indicate the origin of the analyzed crystals. (2) Swiss Alps.

in comparison with the data available in the literature. The data from this study show a better-constrained value of the shape parameter, which is in the highly oblate area.

6. Discussion

Single crystal anisotropies are presented for biotite, muscovite and chlorite in which the paramagnetic component has been isolated using a high-field torque magnetometer. The paramagnetic anisotropy of both micas and chlorite is highly oblate (Figs. 3, 7 and 8). The orientation of the paramagnetic ellipsoid is consistent with the crystallographic structure of phyllosilicates. The k_3 axes are subparallel to the crystallographic *c*-axes in all three minerals (Fig. 9a and b). The deviation between the two minimum susceptibility axes is never higher than 9° in samples with no significant ferromagnetic contribution to the anisotropy (Fig. 9c). This has been confirmed independently in the case of biotite single crystals where the susceptibility was measured within the basal plane. Interaction between the layers in the phyllosilicate structure would cause deviation of the minimum susceptibility axes away from the vertical due to the shift in cation position with respect to adjacent sheets. The orientation of maximum and intermediate axes of susceptibility with respect to the crystallographic axes could not be established within the accuracy of the measurements. However, the specific measurements done in the basal plane suggest that the susceptibility is isotropic.

In those samples where the ferrimagnetic anisotropy fraction was statistically significant in the torque measurements, a general pattern that governs the orientation of the ferrimagnetic tensor with respect to the crystal orientation could not always be found (Fig. 9b). The differences between the minimum susceptibility directions reached 109° in some samples (Fig. 9c). This lack of correspondence has important implications for thermal enhancement of magnetic fabrics. It has been suggested that by heating rocks above 500–600 °C, new ferrimagnetic phases will be generated that mimic the fabric of phyllosilicates (Borradaile and Lagroix, 2000; Trindade et al., 2001). The results from this study indicate that new ferrimagnetic phases may not necessarily nucleate in the direction of the silica lattice (Trindade et al., 2001).

The degree of anisotropy of the paramagnetic fraction in biotites is similar to previously reported

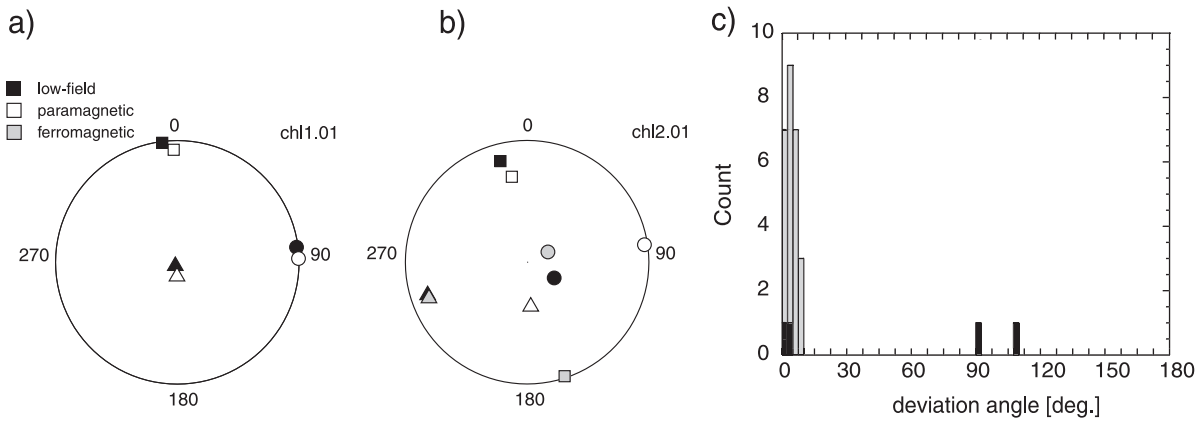

Fig. 9. (a) Relationship between the principal directions of the low-field AMS and the paramagnetic susceptibility principal directions in a chlorite sample without significant ferromagnetic contribution to the magnetic anisotropy. The crystallographic *c*-axis is oriented parallel to the *y*-axis direction in this and next figure. (b) Relationship between the principal directions of the low-field AMS, the paramagnetic anisotropy susceptibility, and the ferromagnetic susceptibility principal directions in a sample with significant ferromagnetic contribution to the magnetic anisotropy. (c) Histogram with the deviation angle between the minimum susceptibility semiaxis measured by low-field methods and the paramagnetic component of the high-field method. Gray bars indicate samples without significant contribution to the anisotropy and black bars indicate samples with significant ferromagnetic contribution to the anisotropy.

data. The values still show some variability. One possible explanation is that the crystals have variable iron content or variable Fe^{2+}/Fe^{3+}, as has been confirmed by preliminary Mössbauer spectra (Table 1). The values for the iron content obtained in Mössbauer measurements reflect a bulk variation in the cation content. For the four samples that were analyzed, there appears to be a relationship between Fe^{2+}/Fe^{3+} and the degree of anisotropy. Further crystals would need to the evaluated to confirm if the variability in P_j can be related to this ratio. In the case of muscovite and chlorite, the anisotropy degree is smaller than values reported previously (Figs. 7 and 8). The differences in the anisotropy degree between biotite, which has iron cations in the crystallographic structure, and muscovite and chlorite in which iron is a product of substitution, were not large. The values presented here suggest these differences are due to compositional variations.

Almost all our samples contained ferrimagnetic inclusions as demonstrated by IRM acquisition curves. Therefore, some of the differences between our results and those in the literature are due to the fact that the high-field measurements isolate the paramagnetic contribution to susceptibility. Other differences may arise from the small size of the samples required when measuring hysteresis curves. These early studies were dependent on measuring magnetization curves along the principal axes of susceptibility, which one must assume is known. A new method proposed by Kelso et al. (2002) that measures magnetization curves in fifteen positions would be an alternative. It does not make any a priori assumption about the orientation of the susceptibility ellipsoid.

7. Conclusions

The paramagnetic anisotropy of biotite, muscovite as well as chlorite has been successfully determined on a collection of samples from different localities. The results presented in this work have two advantages over results previously reported. First, the values were obtained by separation of the paramagnetic component of the crystal from the ferromagnetic component due to impurities. The importance of this separation has been already mentioned by several authors (Borradaile and Werner, 1994; Lagroix and Borradaile, 2000). The separation provides a more accurate value with respect to the low-field methods that measure all the magnetic phases (Borradaile et al., 1987; Zapletal, 1990). Our study also shows a significant improvement in the determination of the AMS ellipsoid with respect to previous values reported by high-field methods (Borradaile and Werner, 1994). The minimum susceptibility axes in all the samples is subparallel to the crystallographic *c*-axis.

The anisotropy degree found for biotite is $P_j = 1.31$, in the range of previously reported values. The shape of the susceptibility ellipsoid is highly prolate with a shape parameter $T = 0.96$. The minimum susceptibility axis is subparallel to the pole to the basal plane, which suggests that there is no interaction between the sheets of the crystal, at least at room temperature.

For muscovite single crystals, the degree of anisotropy has a mean value of $P_j = 1.15$, which is smaller than previously reported values. The shape of the susceptibility ellipsoid is more oblate than other values existing in the literature and has a mean $T = 0.84$. There are notable differences between the paramagnetic bulk susceptibility from crystal to crystal, which influences the determination of the degree of anisotropy. Further analyses are required to examine the effect of cation content on the degree of anisotropy of muscovite. However, with the results obtained on biotites, cation content appears to be important.

In the case of chlorite, it is important to highlight the presence of high coercivity phase in the samples, as seen in the IRM acquisition curves. These samples have been discarded in this analysis, since their torque curves may not be dependent on the square of applied field. The anisotropy degree obtained is smaller than reported previously, and has a mean value of $P_j = 1.15$. However, the values are similar to the low-field values for those samples without a significant ferromagnetic contribution to the anisotropy of magnetic susceptibility. The shape of the susceptibility ellipsoid is highly oblate with a T value of 0.95.

Previous studies have shown that the bulk susceptibility depends on the iron and manganese cations in the crystals, for the particular case of micas (Rochette, 1987; Rochette et al., 1992). Preliminary Mössbauer measurements confirm this relationship and

suggest that also the degree of anisotropy is governed by the cation content. The number of analyzed samples from this study, however, is not large enough to justify statistical analysis. Further work is needed to test this correlation since a dependence of degree of anisotropy on iron content will affect correlations between strain and anisotropy of magnetic susceptibility.

Acknowledgements

This work was supported by the Swiss National Science Foundation, Project no. 21-50639.97. All the samples from the Swiss Alps were kindly provided by Dr. Peter Brack from the collection of the ETH Geology and Mineralogy Museum. We thank Prof. W. Lowrie, Prof. P. Rochette and an anonymous reviewer for the critical reading of the manuscript. R. Egli is gratefully thanked for his patient help in the measurement of our samples. Contribution no. 1276, Institute of Geophysics, ETH Zurich.

References

Ballet, O., Coey, J.M.D., 1982. Magnetic properties of sheet silicates; 2:1 layer minerals. Phys. Chem. Miner. 8, 218–229.

Ballet, O., Coey, J.M.D., Burke, K.J., 1985. Magnetic properties of sheet silicates; 2:1:1 layer minerals. Phys. Chem. Miner. 12, 370–378.

Beausoleil, N., Lavallee, P., Yelon, A., Ballet, O., Coey, J.M.D., 1983. Magnetic properties of biotite micas. J. Appl. Phys. 54 (2), 906–915.

Bergmüller, F., Bärlocher, C., Geyer, B., Grieder, M., Heller, F., Zweifel, P., 1994. A torque magnetometer for measurements of the high-field anisotropy of rocks and crystals. Meas. Sci. Technol. 5, 1466–1470.

Borradaile, G.J., Lagroix, F., 2000. Thermal enhancement of magnetic fabric in high grade gneisses. Geophys. Res. Lett. 27 (16), 2413–2416.

Borradaile, G.J., Werner, T., 1994. Magnetic anisotropy of some phyllosilicates. Tectonophysics 235, 223–248.

Borradaile, G.J., Mothersill, J., Tarling, D., Alford, C., 1985. Sources of magnetic susceptibility in a slate. Earth Planet. Sci. Lett. 76, 336–340.

Borradaile, G.J., Keeler, W., Alford, C., Sarvas, P., 1987. Anisotropy of magnetic susceptibility of some metamorphic minerals. Phys. Earth Planet. Inter. 48, 161–166.

Cheeney, R.F., 1983. Statistical Methods in Geology. George Allen & Unwin, London. 169 pp.

de Wall, H., Bestmann, M., Ullemeyer, K., 2000. Anisotropy of diamagnetic susceptibility in Tassos marble: a comparison between measured and modeled and modeled data. J. Struct. Geol. 22, 1761–1771.

Deer, W.A., Howie, R.A., Zussman, J., 1975. An Introduction to the Rock Forming Minerals. Longman, London. 528 pp.

Dunlop, D.J., Özdemir, Ö., 1997. Rock Magnetism. Cambridge Univ. Press, Cambridge. 573 pp.

Hirt, A.M., Lowrie, W., Clendenen, W.S., Kligfield, R., 1993. Correlation of strain and the anisotropy of magnetic susceptibility in the Onaping formation: evidence for a near-circular origin of the Sudbury basin. Tectonophysics 225, 231–254.

Hirt, A.M., Julivert, M., Soldevila, J., 2000. Magnetic fabric and deformation in the Navia-Alto Sil slate belt, Northwestern Spain. Tectonophysics 320, 1–16.

Hood, W.C., Custer, R.L.P., 1967. Mass magnetic susceptibilities of some trioctahedral micas. Am. Mineral. 52, 1643–1648.

Jelinek, V., 1978. Statistical processing of magnetic susceptibility measured on groups of specimens. Stud. Geophys. Geod. 22, 50–62.

Jelinek, V., 1981. Characterization of the magnetic fabric of rocks. Tectonophysics 79, T63–T67.

Kelso, P.R., Tikoff, B., Jackson, M., Sun, W., 2002. A new method for the separation of paramagnetic and ferromagnetic susceptibility anisotropy using low field and high field methods. Geophys. J. Int. 151, 345–359.

Lagroix, F., Borradaile, G., 2000. Magnetic fabric interpretation complicated by inclusions in mafic silicates. Tectonophysics 325, 207–225.

Lalonde, A.E., Rancourt, D.G., Ping, J.Y., 1998. Accuracy of ferric/ferrous determinations in micas: a comparison of Mössbauer spectroscopy and the Pratt and Wilson wet-chemical methods. Hyperfine Interact. 117, 175–204.

Lüneburg, C.M., Lampert, S.A., Lebit, H.K., Hirt, A.M., Casey, M., Lowrie, W., 1999. Magnetic anisotropy, rock fabrics and finite strain in deformed sediments of SW Sardinia (Italy). Tectonophysics 307, 51–74.

Martín-Hernández, F., Hirt, A.M., 2001. Separation of ferrimagnetic and paramagnetic anisotropies using a high-field torsion magnetometer. Tectonophysics 337, 209–221.

Muxworthy, A.R., 1999. Low-temperature susceptibility and hysteresis of magnetite. Earth Planet. Sci. Lett. 169, 51–58.

Parry, G.R., 1971. The Magnetic Anisotropy of Some Deformed Rocks. PhD Thesis, University of Birminham. 189 pp.

Porath, H., Chamalaun, F.H., 1966. The magnetic anisotropy of hematite bearing rocks. Pure Appl. Geophys. 67, 81–88.

Rancourt, D.G., 1998. Mössbauer spectroscopy in clay science. Hyperfine Interact. 117, 3–38.

Rochette, P., 1987. Magnetic susceptibility of the rock matrix related to magnetic fabric studies. J. Struct. Geol. 9, 1015–1020.

Rochette, P., Jackson, M., Aubourg, C., 1992. Rock magnetism and the interpretation of anisotropy of magnetic susceptibility. Rev. Geophys. 30, 209–226.

Siegesmund, S., Ullemeyer, K., Dahms, M., 1995. Control of magnetic rock fabrics by mica preferred orientation: a quantitative approach. J. Struct. Geol. 17 (11), 1601–1613.

Syono, Y., 1960. Magnetic susceptibility of some rock forming

silicate minerals such as amphiboles, biotites, cordierites and garnets. J. Geomagn. Geoelectr. 12, 85–93.

Tarling, D.H., Hrouda, F., 1993. The Magnetic Anisotropy of Rocks. Chapman & Hall, London. 217 pp.

Townsend, M.G., Longworth, G., 1985. Sign of the magnetic coupling of Fe^{2+} and Fe^{3+} in biotite. Phys. Chem. Miner. 12, 141–144.

Trindade, R.I.F., Mintsa Mi Nguema, T., Bouchez, J.L., 2001. Thermally enhanced mimetic fabric of magnetite in a biotite granite. Geophys. Res. Lett. 28 (14), 2687–2690.

Verwey, E.J., 1939. Electronic conduction of magnetite (Fe_3O_4) and its transition point at low temperature. Nature 144, 327–328.

Zapletal, K., 1990. Low-field susceptibility anisotropy of some biotite crystals. Phys. Earth Planet. Inter. 63, 85–97.